UCLA
COMPUTATIONAL AND APPLIED MATHEMATICS

Power-Law Starting Flow Past a Flat Plate: Brown and Michael's Model, Scaling, and Universality

L. Cortelezzi

April 1995

CAM Report 95-20

Department of Mathematics
University of California, Los Angeles
Los Angeles, CA. 90024-1555

Power-law starting flow past a flat plate: Brown and Michael's model, scaling, and universality.

by L. CORTELEZZI*

April 19, 1995

Abstract

Two-dimensional unsteady separated flow past a flat plate is considered. The rolling-up of the separated shear-layer is modelled by a pair of point vortices whose time-dependent circulation is predicted by an unsteady Kutta condition. A power-law starting flow is assumed and the model is validated. The evolution of the characteristic quantities of the flow is presented. Two time-dependent scalings which respectively capture the universality of the flow at early and at large times are proposed. The results obtained for the scaled system are presented. The possibility of scaling the corresponding viscous flow is discussed.

*Department of Mathematics, University of California, Los Angeles, California 90024-1555, E-mail: crtlz@math.ucla.edu

1 Introduction

The process of nondimensionalizing the appropriate equations of fluid dynamics is commonly used to present the results of certain physical phenomenon in terms of the least number of parameters. In the particular case of incompressible steady flow past a bluff body the dimensionless variables are obtained by scaling the physical variables with an appropriate combination of characteristic length and time. The characteristic length might be some linear dimension of the body and the characteristic time is usually derived by taking the ratio of the characteristic length with the characteristic velocity, i.e., with the undisturbed free-stream velocity. When this class of flows is described by the Navier-Stokes equations, the scaling process produces only one dimensionless parameter: the Reynolds number. Then all flows with the same Reynolds number and geometry are said dynamically similar. The principle of dynamical similarity is commonly used to obtain information about an unknown flow field from experiments carried out under more convenient physical conditions than those of the unknown flow field.

A question rises if it is possible to apply this frame work to flow fields where the free-stream velocity is time varying. The answer is positive only under certain conditions when, for example, the free-stream velocity oscillates with fixed amplitude and frequency about a mean value. In this case the scaling process which makes the incompressible flow past an oscillating body dimensionless generates two parameters: the Reynolds and the Strouhal numbers. When, instead, the free-stream velocity does not present any physically meaningful periodicity nor a mean value, a power of time in the simplest case, it is not possible to achieve dynamical similarity by scaling the problem using characteristic length and velocity.

In exceptional cases the scaling process produces a result even stronger than dynamical similarity: Universality. The concept of universality, which recently became popular in connection with the idea of self-organized criticality, simply states that certain physical phenomena present the same behavior when scaled properly. The aim of this paper is to achieve dynamical similarity and furthermore, universality, by scaling the power-law starting flow past a flat plate with characteristic quantities which are function of time. In other words, we intend to show that all the results for a given flow quantity may be collapsed on a unique curve, which is hence universal, when the mathematical problem is scaled with an appropriate function of time.

The study of power-law starting flow past a flat plate at high Reynolds numbers might be approached theoretically by using two different inviscid models. In the simpler case the rolling up of the separated shear layer could be modelled by a point vortex with time varying circulation (Brown and Michael 1954, Rott 1956, Cortelezzi and Leonard 1993) while in a more sophisticated approach a continuous vortex sheet could be used (Rott1956, Pullin 1978). A comparison between the two methods when used to model the unsteady separated flow past a semi-infinite plate has been presented by Pullin and by Cortelezzi and Leonard. As shown by the author (Cortelezzi and Leonard 1993) the two models lead to the same power-law solution with slightly different coefficients when the free-stream velocity follows also a power-law. We assume similar general agreement for

the present study of power-law starting flow past a flat plate and therefore use the simpler point vortex model.

In Section 2, following our previous work (Cortelezzi and Leonard 1993), we model the unsteady separation from the tips of a flat plate by means of a pair of point vortices whose time-dependent circulation is predicted by an unsteady Kutta condition. The problem is further simplified by imposing wake symmetry. The motion of the vortex pair is determined by a non-linear ordinary differential equation first proposed by Brown and Michael in 1954. In Section 3, making the problem dimensionless we find there does not exist a characteristic velocity for this class of flows yielding dynamical similarity. Dimensional analysis, however, permits us to derive a characteristic time scale from the power-law form of the free-stream velocity. Making the problem dimensionless using such a characteristic quantity we achieve the dynamical similarity for a given power-law exponent. Then the model is tested simulating the separated flow when the free-stream is a step, or a linear or a parabolic function of time and finally the model is validated matching the results obtained both numerically and experimentally for the first two cases.

In Section 4, analyzing the results obtained we observe that the vortices always move on the nearly same trajectory and that the geometry of the flow, i.e., critical points and separatrix, seems also to develop in a similar fashion but, of course, the corresponding time differs depending on the power-law of the free-stream velocity. All these facts suggest the existence of a further time-dependent scaling which unveils the universality of the phenomenon, i.e., a scaling which collapses all the results for a certain flow quantity onto a universal curve. We derive a time-dependent scaling by synchronizing the motion of the plate for different time-laws. The resulting equation of motion for the vortex pair is, for large times, independent of all the flow parameters and hence universal. All the characteristic quantities of the flow are recomputed. These results, in addition to capturing the universality of the flow for large times, also point to a universality for early times of the wake evolution, i.e., when the plate has traveled few plate lengths or less.

In Section 5, we first obtain the equation of motion for the starting vortex which models the separation of a flow past a semi-infinite plate. We analytically solve this equation for a generic free-stream velocity and then we deduce a time-dependent scaling which captures the universality of this flow. Under this time scaling the exact solution for any free-stream velocity reduces to the exact solution for the impulsively started case. Finally, the comparison between the scaling obtained for the semi-infinite case, which holds at the very early times of the flow past a finite plate, and the scaling derived for large times suggests a more complicated time-dependent scaling effective in the early times of the power-law flow past a flat plate. All the results scaled in this fashion nearly collapse onto the corresponding curve for the impulsively started case which is hence universal. We conclude our study by discussing the possibility of scaling the corresponding viscous flow.

2 Mathematical formulation

In this section we introduce a mathematical model able to represent the two dimensional unsteady separation from the tips of a finite plate normal to an unsteady free-stream velocity. We restrict

our investigation to the cases where the regions of vorticity that separate from the boundary layer and are convected away are thin enough to justify a description by mean of a vortex sheet. The consequent stretching and rolling up of the vortex sheet suggests to replace the spirals with point vortices. However, the vortex sheet is not completely lost, it is assumed of negligible circulation. It connects the feeding point to a point vortex of variable strength which replaces the core of the forming spiral and satisfies an unsteady Kutta condition. Mathematically the feeding vortex sheet is just the branch cut due to the logarithmic singularity representing the vortex.

The mathematical formulation of the problem can be simplified by choosing a frame of reference fixed to the plate so that the body can be identified with the segment $[-2ia, 2ia]$. Then, the flow of an incompressible irrotational fluid about such a body can be solved via conformal mapping. The Joukowski transformation, which maps a finite plate of length $L = 4a$ in the z-plane onto the circle of radius a in the ζ-plane (see Figure 1a) and preserves the characteristic of the flow at infinity, has the following form:

$$z = \zeta - \frac{a^2}{\zeta}. \tag{1}$$

There is experimental evidence (Taneda and Honji 1971, Lisoski 1993) that the near wake is nearly two dimensional and symmetric about the x-axis during the early times of the flow and such a condition is enhanced when the plate moves with a non-zero acceleration. Under these circumstances the problem can be further simplified imposing symmetry with respect to the real axis, i.e., the vortices have equal and opposite circulation, Γ_1 and $-\Gamma_1$, and are located in complex conjugate positions, ζ_1 and $\bar{\zeta}_1$, respectively. Since the velocity field has to satisfy Laplace's equation and the boundary condition in the mapped plane can be treated using the circle theorem, we can build the complex potential F superimposing basic flows. Thus, the complex velocity field $w = \frac{dF}{d\zeta}$ has the form:

$$w(\zeta, t) = U\left(1 - \frac{a^2}{\zeta^2}\right) + \frac{i\Gamma_1}{2\pi}\left(\frac{1}{\zeta - \zeta_1} + \frac{\bar{\zeta}_1}{a^2 - \zeta\bar{\zeta}_1} - \frac{1}{\zeta - \bar{\zeta}_1} - \frac{\zeta_1}{a^2 - \zeta\zeta_1}\right). \tag{2}$$

Note that for convenience we are departing from the usual convention and taking the circulation positive when in the clockwise sense. We impose the Kutta condition to regularize the potential flow at the tips of the plate. In the ζ-plane the flow is non-singular since the singularity has been absorbed by the mapping. To remove the singularity in the z-plane the complex velocity (2) in the mapped plane has to be zero at the top and bottom of the circle, i.e., at $\zeta = \pm ia$. Solving for Γ_1 we obtain:

$$\Gamma_1 = -2\pi i \frac{(a^2 + \zeta_1^2)(a^2 + \bar{\zeta}_1^2)}{(\zeta_1 - \bar{\zeta}_1)(a^2 - \zeta_1\bar{\zeta}_1)} U. \tag{3}$$

Note that the circulation associated with the vortex pair depends on all the flow quantities, i.e., free-stream velocity U, circle radius a, and position of the vortex pair itself. To describe the motion of the vortex pair in the physical plane we use the following ordinary differential equation:

$$\frac{d\bar{z}_1}{dt} + (\bar{z}_1 + 2ia)\frac{1}{\Gamma_1}\frac{d\Gamma_1}{dt} = \lim_{z \to z_1}\left\{\frac{d}{dz}\left[F - \frac{i\Gamma_1}{2\pi}\log(z - z_1)\right]\right\}, \tag{4}$$

with the initial condition:

$$z_1(0) = 2ia. \tag{5}$$

The term containing $\frac{d\Gamma_1}{dt}$ is known as "Brown and Michael's correction". The motion of the vortex of variable strength described by this equation guarantees no net force on the vortex and its connecting cut. The limit on the right hand side, which represents the complex velocity at the vortex location without the self-induced contribution, produces the so called "Routh's correction" (e.g. Clements 1973) when it is evaluated in the mapped plane.

We solve the problem in the mapped plane. Once we have performed the change of variables, substituted for the complex potential and, carried out the limit required in the equation (4), we obtain:

$$\begin{aligned}\left[\frac{\bar{\zeta}_1^2+a^2}{\bar{\zeta}_1^2}+\frac{(\bar{\zeta}_1+ia)^2}{\bar{\zeta}_1}\frac{(a^2+\zeta_1^2)(a^2-\bar{\zeta}_1^2)}{(a^2+\bar{\zeta}_1^2)(\zeta_1-\bar{\zeta}_1)(a^2-\zeta_1\bar{\zeta}_1)}\right]\frac{d\bar{\zeta}_1}{dt} \\ -\left[\frac{(\bar{\zeta}_1+ia)^2}{\bar{\zeta}_1}\frac{(a^2-\zeta_1^2)(a^2+\bar{\zeta}_1^2)}{(a^2+\zeta_1^2)(\zeta_1-\bar{\zeta}_1)(a^2-\zeta_1\bar{\zeta}_1)}\right]\frac{d\zeta_1}{dt} = \\ \left(\frac{\zeta_1^2}{a^2+\zeta_1^2}\right)\left\{U\left(1-\frac{a^2}{\zeta_1^2}\right)+\frac{i\Gamma_1}{2\pi}\left[\frac{\bar{\zeta}_1}{a^2-\zeta_1\bar{\zeta}_1}-\frac{1}{\zeta_1-\bar{\zeta}_1}-\frac{\zeta_1}{a^2-\zeta_1^2}\right]+\frac{i\Gamma_1}{2\pi}\frac{a^2}{\zeta_1(a^2+\zeta_1^2)}\right\} \\ -\frac{(\bar{\zeta}_1+ia)^2}{\bar{\zeta}_1}\frac{1}{U}\frac{dU}{dt},\end{aligned} \tag{6}$$

and the initial condition is

$$\zeta_1(0)=ia, \tag{7}$$

where Γ_1 is given by (3). Because of the size and complexity of the problem we are not attempting an analytical solution, instead, we are proceeding with a numerical integration. Since the equation of motion is singular at time $t=0$ we derive an approximate solution valid for small times following the same procedure presented in our work on the flow past a semi-infinite plate (see Cortelezzi and Leonard 1993). With this solution available we integrate numerically the above equation using a modified Runge-Kutta-Feldberg scheme.

The forces acting on the plate are of particular interest because they can be measured experimentally and are the crucial quantities in any problem involving the interaction between fluids and structures. The forces can be computed by means of the Blasius theorem:

$$D-iL=\frac{1}{2}i\rho\oint_C\left(\frac{dF}{dz}\right)^2dz-i\rho\frac{\partial}{\partial t}\oint_C\bar{F}d\bar{z}. \tag{8}$$

The evaluation of these integrals can be made relatively simple by a careful choice of the integration path C. Since by construction the vortices cannot sustain any force then the forces acting on the plate are the same as the forces acting on the entire system constituted by plate plus vortices and the contour C can be taken around the full system. Because all the singularities are inside the integration path the contour can be stretched to a circle of infinite radius by means of the Cauchy theorem and the forces can be computed using the theorem of the residues.

The integration can be carried out successfully in the mapped plane and the drag has the following form:

$$D=4\pi\rho a^2\frac{dU}{dt}+i\rho\frac{d}{dt}\left[\frac{\Gamma_1(a^2-\zeta_1\bar{\zeta}_1)(\zeta_1-\bar{\zeta}_1)}{\zeta_1\bar{\zeta}_1}\right]. \tag{9}$$

The component of the force along the imaginary axis is zero because of the imposed symmetry. The above expression agrees with those obtained by Cheers (1978) and by Graham (1980). The first

term on the right hand side is the force due to added mass, i.e., is the inertia of the attached flow, while the second term is the contribution due to the evolution of the wake. It is also possible to write the drag as the time derivative of the total impulse, i.e. $D = \frac{dI}{dt}$ where

$$I = 4\pi\rho a^2 U + i\rho\left[\frac{\Gamma_1(a^2 - \zeta_1\bar{\zeta}_1)(\zeta_1 - \bar{\zeta}_1)}{\zeta_1\bar{\zeta}_1}\right]. \tag{10}$$

The last expression represents the impulse required to set up the irrotational flow instantaneously from rest.

3 Nondimensionalization and validation of the model

To make the problem dimensionless we have to define a characteristic length and time. As a representative length we choose, for simplicity, the radius of the circle in the mapped plane. A characteristic velocity, in general, cannot be recognized when the free-stream velocity depends on time. Nevertheless, a characteristic time T can be constructed using one or more parameters present in variation of the free-stream velocity with time. Then all the quantities involved in the problem can be made dimensionless as follows:

$$\begin{aligned} z_1^* &= \frac{z_1}{a}, & \zeta_1^* &= \frac{\zeta_1}{a}, & a^* &= 1, & t^* &= \frac{t}{T}, \\ U^* &= \frac{TU}{a}, & \Gamma_1^* &= \frac{T\Gamma_1}{a^2}, & I^* &= \frac{TI}{\rho a^3}. \end{aligned} \tag{11}$$

Substituting the starred quantities into the equation of motion (6) and simplifying we obtain:

$$\begin{aligned} &\left[\frac{\bar{\zeta}_1^{*2}+1}{\zeta_1^{*2}} + \frac{(\bar{\zeta}_1^*+i)^2}{\bar{\zeta}_1^*}\frac{(1+\zeta_1^{*2})(1-\bar{\zeta}_1^{*2})}{(1+\bar{\zeta}_1^{*2})(\zeta_1^*-\bar{\zeta}_1^*)(1-\zeta_1^*\bar{\zeta}_1^*)}\right]\frac{d\bar{\zeta}_1^*}{dt^*} \\ &\qquad - \left[\frac{(\bar{\zeta}_1^*+i)^2}{\bar{\zeta}_1^*}\frac{(1-\zeta_1^{*2})(1+\bar{\zeta}_1^{*2})}{(1+\zeta_1^{*2})(\zeta_1^*-\bar{\zeta}_1^*)(1-\zeta_1^*\bar{\zeta}_1^*)}\right]\frac{d\zeta_1^*}{dt^*} = \\ &\left(\frac{\zeta_1^{*2}}{1+\zeta_1^{*2}}\right)\left\{U^*\left(1-\frac{1}{\zeta_1^{*2}}\right) + \frac{i\Gamma_1^*}{2\pi}\left[\frac{\bar{\zeta}_1^*}{1-\zeta_1^*\bar{\zeta}_1^*} - \frac{1}{\zeta_1^*-\bar{\zeta}_1^*} - \frac{\zeta_1^*}{1-\zeta_1^{*2}}\right] + \frac{i\Gamma_1^*}{2\pi}\frac{1}{\zeta_1^*(1+\zeta_1^{*2})}\right\} \\ &\qquad - \frac{(\bar{\zeta}_1^*+i)^2}{\bar{\zeta}_1^*}\frac{1}{U^*}\frac{dU^*}{dt^*}, \end{aligned} \tag{12}$$

where

$$\Gamma_1^* = -2\pi i\frac{(1+\zeta_1^{*2})(1+\bar{\zeta}_1^{*2})}{(\zeta_1^*-\bar{\zeta}_1^*)(1-\zeta_1^*\bar{\zeta}_1^*)}U^*, \tag{13}$$

and the initial condition is

$$\zeta_1^*(0) = i. \tag{14}$$

When the free-stream velocity is a power-law, i.e., $U(t) = Vt^m$, we choose the following characteristic time:

$$T = \left(\frac{a}{V}\right)^{\frac{1}{m+1}}, \qquad \forall m \in [0,\infty). \tag{15}$$

Consequently, the dimensionless free-stream velocity and the ratio between acceleration and velocity reduce to $U^* = t^{*m}$ and $\frac{1}{U^*}\frac{dU^*}{dt^*} = m/t^*$, respectively. The problem is now parameterized only by m,

i.e., by the exponent of the free-stream velocity. In other words, for a given m, all the problems are dynamically similar to the one where V and a are unit. Note we recover the usual dimensionless flow quantities in the impulsively started case ($m = 0$) because, in this case, a characteristic free-stream velocity exists.

An opportunity to validate this model is given by the experiment done by Taneda and Honji in 1971. In this experiment they measured the length L_{bbl} of the symmetric wake bubble behind a flat plate impulsively started or constantly accelerated, i.e., when $U(t) = Vt^m$ with $m = 0, 1$. They showed that the growth of the bubble follows a power-law independently of the Reynolds number. When the plate is impulsively started the time law is:

$$\frac{L_{bbl}}{L} = 0.89 \left[\frac{Vt}{L}\right]^{\frac{2}{3}}, \tag{16}$$

while for the constantly accelerated case is:

$$\frac{L_{bbl}}{L} = 0.48 \left[\frac{Vt^2}{L}\right]^{\frac{2}{3}}. \tag{17}$$

Using our vortex model we determine the growth of the recirculating bubble and also compute the position of the stagnation points to obtain a complete characterization of the flow. At early time the flow is characterized by two small recirculating bubbles close to the tips of the plate and three stagnation points can be recognized on the back face of the body (see Figures 5a and b). The stagnation point on the front face of the plate coincides with the origin. Later, as the two recirculating bubbles grow the two stagnation points move away from the tips until they meet at the origin. At this point the two bubbles begin to merge and a new stagnation point is created and moves away from the origin along the positive x-axis (see Figures 5c and d). The merging process is rather sudden and soon a large recirculating bubble dominates the flow (see Figures 5e and f). The length of the bubble is defined as the stream-wise length of the recirculating domain. We say, for convenience, that the merging process is completed at the time when the distance from the stagnation point on the x-axis and the plate becomes the bubble length.

Let us start by computing the positions of the stagnation points on the back face of the plate. They can be determined, in the mapped plane, by the points where the complex velocity w is identically zero along the circle. One point is trivially determined by the intersection of the circle with the x-axis, while the other two points are identified in terms of polar coordinates as follow:

$$\rho^* = 1, \qquad \theta^* = \pm \arcsin\left[\frac{(\rho_1^{*2} + 1)\sin\theta_1^*}{\rho_1^*}\right], \tag{18}$$

where $\zeta^* = \xi^* + i\eta^* = -i\rho^* e^{i\theta^*}$, (see Figure 1a). The position of these points in the physical plane can be determined using the mapping (1):

$$x^*_{stgp} = 0^+, \qquad y^*_{stgp} = \pm\frac{2}{\rho_1^*}\sqrt{\rho_1^{*2} - (\rho_1^{*2} + 1)^2 \sin^2\theta_1^*}. \tag{19}$$

where $z^* = x^* + iy^*$.

Now we consider the stagnation points on the x-axis. They can be identified with the points where the real part of the complex velocity field is zero. The non trivial point created by the merging of the two bubbles has the following position in the mapped plane:

$$\xi^* = \frac{\sqrt{(\rho_1^{*2}+1)^2 \sin^2\theta_1^* - \rho_1^{*2}} + (\rho_1^{*2}+1)\sin\theta_1^*}{\rho_1^*}, \qquad \eta^* = 0. \tag{20}$$

As before, the position of this point in the physical plane can be determined using the mapping (1).

$$x^*_{stgx} = \frac{2}{\rho_1^*}\left[\frac{(\rho_1^{*2}+1)\sin\theta_1^*\sqrt{(\rho_1^{*2}+1)^2\sin^2\theta_1^* - \rho_1^{*2}} + (\rho_1^{*2}+1)^2\sin^2\theta_1^* - \rho_1^{*2}}{\sqrt{(\rho_1^{*2}+1)^2\sin^2\theta_1^* - \rho_1^{*2}} + (\rho_1^{*2}+1)\sin\theta_1^*}\right], \qquad y^*_{stgx} = 0. \tag{21}$$

Note that the evolution of the flow depends on the sign of the following expression:

$$(\rho_1^{*2}+1)^2\sin^2\theta_1^* - \rho_1^{*2}. \tag{22}$$

The above quantity is negative at the early stages of the flow when there are two small recirculating bubbles and consequently the expressions (18) and (19) are well defined. Later, when the bubbles meet at the origin the quantity (22) is zero and the stagnation points defined by (19) and (21) coincide. Finally, as the merging process takes place the above quantity turns positive and the expressions (20) and (21) become well defined. It is interesting to observe that all the above expressions (18–22) are independent of the free-stream velocity $U(t)$ and the circulation $\Gamma_1(t)$ and the only important information is the position of the vortex pair. This fact suggests that the entire geometry of the flow might evolve independently of the time-dependence of $U(t)$ and $\Gamma_1(t)$.

The length of the recirculating bubble can be mathematically identified with the real part of the solution of the following two equations:

$$\Im(F^*) = 0, \qquad \Re(\frac{dF^*}{dz^*}) = 0, \tag{23}$$

where $\Re$ and $\Im$ indicate the real and imaginary part, respectively. The solution of this set of equations is a point which lies on the zero streamline, the one that separates the recirculating region from the rest of the flow, where the complex velocity field is parallel to the plate. Note as the merging process is completed this statement becomes trivial and this point becomes the stagnation point x^*_{stgx} defined by the expression (21). At earlier time the solution of this problem is not trivial but it can be obtained numerically.

The numerical simulation of the power-law starting flow past a flat plate in illustrated by Figures 2a-d. These plots permit the comparison of the cases where the plate is impulsively started, constantly accelerated and linearly accelerated, i.e., when $U(t) = Vt^m$ with $m = 0, 1, 2$. A striking feature is that each vortex moves on nearly the same trajectory in all three cases (see Figure 2a). Figures 2b-d show the total circulation and rate of circulation production for the top vortex, and the total impulse. The small window magnifies the trend at small times when it is comparable with the results obtained for the semi-infinite plate (see Cortelezzi and Leonard 1993).

Figure 3 shows how the length of the recirculating bubble for the impulsively started case compares with the best fit (16) presented by Taneda and Honji (1971) and with that computed by

Chua (1990). Note that Chua in his simulation uses a vortex method algorithm able to model the boundary layer on the plate and represent the distributed vorticity in the wake. The agreement is reasonably good but both numerical simulations show a similar departure from the best fit proposed by Taneda and Honji. At small times, we are able to extend Taneda and Honji's result down to time $Vt/L \sim O(10^{-7})$. We estimate that at very early times ($10^{-7} < Vt/L < 10^{-5}$, not shown in the figure) the bubble grows proportionally to $(Vt/L)^{0.68}$, which is in good agreement with time-law of $(Vt/L)^{\frac{2}{3}}$ derived by Pullin for the semi-infinite plate case (see Pullin 1978). This time-law slightly changes with time, as the coupling between top and bottom vortices becomes more important. In fact, during the merging process ($0.15 < Vt/L < 1.5$) we estimate that the bubble grows as $(Vt/L)^{0.77}$. Later, the departure from the quasi-linear trend, in the log-log plot, can be clearly identified with the end of the merging process. See the solid diamond symbol. Finally, for large times the deviation from the experiment is not anymore negligible but consistent with the other numerical simulation. This departure could be consequence of the two-dimensionality and symmetry imposed in our model and two-dimensionality in Chua's calculation or finite Reynolds number effect in the experiment.

The forces acting on the plate for the purely impulsively started case cannot be measured experimentally. However, a comparison can be made with the results obtained by Chua (1990) in his numerical simulation (see Figure 4a), where the drag coefficient is defined as $C_D = D/2\rho U^2 L$. The overall agreement is reasonably good. Figure 3 shows that the recirculating bubble grows faster in Chua's simulation than in our case and this explains the difference in drag at early times. At later times our model tends to underestimate the drag probably because of the lack of distributed vorticity and imposed symmetry.

When the plate is uniformly accelerated the forces can be measured experimentally. Results for the drag are not available from Taneda and Honji's (1971) experiment, but recently Lisoski (1993) measured the forces acting on a uniformly accelerated flat plate. Figure 4b shows the comparison with Lisoski and Chua (1990) results. The overall agreement is still reasonably good and the discrepancies can be explained as for the impulsively started case. Note the drag coefficient, in this case, is based on the final free-stream velocity.

4 Scaling at Large Times

In this section we derive a time-dependent scaling which will generate a family of similar curves for each flow quantity, allowing one to compare results for different time laws. Clearly the geometrical scaling (11) introduced to make the problem dimensionless fails this purpose. However, if we analyze the plots presented in the previous section we note some striking results. First, the vortex pair moves on nearly the same trajectory independently of the time law for the free-stream velocity (see Figure 2a). Furthermore, from the comparison of the instantaneous streamlines taken at two different times for two different free-stream conditions (see Figures 5a-f), it follows that the geometry of the flow goes through the same states but at different times. Finally, the scaling used by Taneda and Honji (1971) seems to be appropriate for the analysis of this flow.

Based on the above observations it follows that the appropriate choice of a representative time scale it would improve the quantitative and qualitative understanding of the phenomenon. If we divide the equation of motion (12) for the power-law case by t^{*m} we obtain terms containing $t^{*(m+1)}$ or $t^{*m}dt^*$ which suggest that the time scaling should be $\sim t^{*(m+1)}$ or, in other words, the scaling should involve the distance traveled by the plate. This distance, x_p, can be easily computed by integrating the free-stream velocity over time. Then, the number of radii traveled by the plate when the free-stream velocity is a power-law is:

$$\frac{x_p}{a} = \frac{V t^{m+1}}{a(m+1)}. \tag{24}$$

Thus, if we choose the right hand side as the dimensionless time, then the motion of the plate is synchronized in this new time frame. In other words, the plate travels an equal distance in time for all possible free-stream conditions (i.e.$\forall m \in [0, \infty)$).

Because of the considerations above, it is natural to introduce the following scaled quantities:

$$\begin{aligned} z_1^\bullet &= z_1^*, & \zeta_1^\bullet &= \zeta_1^*, & a^\bullet &= a^*, & t_L^\bullet &= \frac{t^{*(m+1)}}{m+1}, \\ U^\bullet &= \frac{U^*}{t^{*m}} = 1, & \Gamma_1^\bullet &= \frac{\Gamma_1^*}{t^{*m}}, & I^\bullet &= \frac{I^*}{t^{*m}}, \end{aligned} \tag{25}$$

where the subscript L stands for "large times". A consequence of this time dependent scaling is that the quantities which involve time derivatives have a non trivial and rather unusual expression. Let g represent Γ_1 or I, then the expression for the scaled rate of circulation production and drag can be obtained from the following formula:

$$\frac{dg^\bullet}{dt_L^\bullet} = \frac{1}{t^{*2m}}\left(\frac{dg^*}{dt^*} - \frac{mg^*}{t^*}\right). \tag{26}$$

Note for $m = 0$ we recover the geometrical scaling (11). Rewriting the equation of motion (12) for the power-law case in terms of these scaled quantities, we obtain:

$$\begin{aligned} &\left[\frac{\bar{\zeta}_1^{\bullet 2}+1}{\bar{\zeta}_1^{\bullet 2}} + \frac{(\bar{\zeta}_1^\bullet + i)^2}{\bar{\zeta}_1^\bullet}\frac{(1+\zeta_1^{\bullet 2})(1-\bar{\zeta}_1^{\bullet 2})}{(1+\bar{\zeta}_1^{\bullet 2})(\zeta_1^\bullet - \bar{\zeta}_1^\bullet)(1-\zeta_1^\bullet\bar{\zeta}_1^\bullet)}\right]\frac{d\bar{\zeta}_1^\bullet}{dt_L^\bullet} \\ &\qquad - \left[\frac{(\bar{\zeta}_1^\bullet + i)^2}{\zeta_1^\bullet}\frac{(1-\zeta_1^{\bullet 2})(1+\bar{\zeta}_1^{\bullet 2})}{(1+\zeta_1^{\bullet 2})(\zeta_1^\bullet - \bar{\zeta}_1^\bullet)(1-\zeta_1^\bullet\bar{\zeta}_1^\bullet)}\right]\frac{d\zeta_1^\bullet}{dt_L^\bullet} = \\ &\left(\frac{\zeta_1^{\bullet 2}}{1+\zeta_1^{\bullet 2}}\right)\left\{\left(1-\frac{1}{\zeta_1^{\bullet 2}}\right) + \frac{i\Gamma_1^\bullet}{2\pi}\left[\frac{\bar{\zeta}_1^\bullet}{1-\zeta_1^\bullet\bar{\zeta}_1^\bullet} - \frac{1}{\zeta_1^\bullet - \bar{\zeta}_1^\bullet} - \frac{\zeta_1^\bullet}{1-\zeta_1^{\bullet 2}}\right] + \frac{i\Gamma_1^\bullet}{2\pi}\frac{1}{\zeta_1^\bullet(1+\zeta_1^{\bullet 2})}\right\} \\ &\qquad - \frac{(\bar{\zeta}_1^\bullet + i)^2}{\bar{\zeta}_1^\bullet}\frac{m}{(m+1)t_L^\bullet}, \end{aligned} \tag{27}$$

where

$$\Gamma_1^\bullet = -2\pi i \frac{(1+\zeta_1^{\bullet 2})(1+\bar{\zeta}_1^{\bullet 2})}{(\zeta_1^\bullet - \bar{\zeta}_1^\bullet)(1-\zeta_1^\bullet\bar{\zeta}_1^\bullet)}, \tag{28}$$

and the initial condition is

$$\zeta_1^\bullet(0) = i. \tag{29}$$

Note that the scaling reduces the dependency from the free-stream velocity to the factor $m/(m+1)$ which appears in the last term of the equation of motion. In other words, the scaled equation is the

dimensionless equation of motion for the impulsively started case plus a correction which dies out at large time because of the factor t_L^{*-1}. Consequently, the scaled equation becomes, for large times, the universal equation of motion because it describes the evolution of the flow independently of all flow parameters. Varying the power of time we produce a family of curves, bounded by the limiting cases $m = 0, \infty$, which can be compared with the impulsively started case as is shown by Figures 6 and 7. Indication of universality is that at large times the curves collapse all together, as in the case for the rate of circulation production and drag (see Figures 6b and d), or they become parallel as in the case of total circulation and total impulse (see Figures 6a and c).

In this time frame, it becomes meaningful to compare the time evolution of the geometrical quantities which characterize the flow (see Figure 7). The bubble length (i.e., the branch of solid curve past the diamond symbol), at any given time, decreases as m increases. The merging process of the two small recirculating bubbles is delayed also as m becomes larger. The diamond symbols in Figure 7 show at which time the merging process is completed. Note that this happens always at about the same bubble length and consequently this length is a universal quantity for this class of flows.

5 Scaling at Early Times

In this section we derive a time dependent scaling which nearly collapses, during the early times of the flow, all the curves for a given flow quantity on the corresponding curve produced by the impulsively started case. As a first step in the derivation we analyze the corresponding separated flow past a semi-infinite plate. We derive the equation of motion for the starting vortex and then we solve the problem in closed form. Finally, we find a time dependent scaling which collapses all the solutions on the solution for the impulsively started case which, consequently, is the universal solution for the semi-infinite plate problem. In the last subsection we extend the scaling derived for the semi-infinite plate to the flow past a finite plate. As before, we are able to nearly collapse all the results onto the corresponding curves obtained for the impulsively started case but only up to the time when the plate has traveled few plate lengths.

5.1 Flow past a semi-infinite plate

5.1.1 Mathematical formulation

The unsteady separated flow past a semi-infinite plate has been studied in details by several authors: Rott 1956, Pullin 1978, and Cortelezzi and Leonard 1993. Following our previous work we map the plate lying on the negative imaginary axis onto the real axis of the mapped plate, see Figure 1b.

Then, the equation of motion for the starting vortex has the following form:

$$\left[2i\bar{\zeta}^*_{1_S} + \frac{i\zeta^*_{1_S}\bar{\zeta}^*_{1_S}}{\zeta^*_{1_S} - \bar{\zeta}^*_{1_S}}\right]\frac{d\bar{\zeta}^*_{1_S}}{dt^*_S} - \left[\frac{i\bar{\zeta}^{*3}_{1_S}}{\zeta^*_{1_S}(\zeta^*_{1_S} - \bar{\zeta}^*_{1_S})}\right]\frac{d\zeta^*_{1_S}}{dt^*_S} = \frac{i}{2\zeta^*_{1_S}}\left[U^*_S - \frac{i\Gamma^*_{1_S}}{2\pi(\zeta^*_{1_S} - \bar{\zeta}^*_{1_S})} - \frac{i\Gamma^*_{1_S}}{4\pi\zeta^*_{1_S}}\right] - i\bar{\zeta}^{*2}_{1_S}\frac{1}{U^*_S}\frac{dU^*_S}{dt^*_S}, \tag{30}$$

where

$$\Gamma^*_{1_S} = 2\pi i\left(\frac{\zeta^*_{1_S}\bar{\zeta}^*_{1_S}}{\zeta^*_{1_S} - \bar{\zeta}^*_{1_S}}\right)U^*_S, \tag{31}$$

and the initial condition is

$$\zeta^*_{1_S}(0) = 0, \tag{32}$$

where $\zeta^*_{1_S}$ is the position of the vortex in the mapped plane, $\Gamma^*_{1_S}$ in the circulation of the vortex, and U^*_S is the free-stream velocity. All the quantities are stared because the problem is intrinsically dimensionless. The subscript S, which stands for "small times", differentiates these variables from the one used for the finite plate problem.

5.1.2 Exact Solution

In this section we derive the exact solution of the equation of motion for the starting vortex (30–32) when the free-stream velocity is positive semi-definite, i.e., $U^*_S \geq 0\ \forall t^*_S \geq 0$. This restriction does not violate the generality of the solution because when the flow reverses the solution cannot be given in terms of only one vortex, as we will prove later in this subsection.

For convenience we rewrite the equations (30) and (32) in polar form (see Figure 1) as follows:

$$\begin{cases} \dfrac{d\rho^*_{1_S}}{dt^*_S} = \dfrac{U^*_S \sin\theta^*_{1_S}}{12\rho^{*2}_{1_S}} - \dfrac{\rho^*_{1_S}}{3U^*_S}\dfrac{dU^*_S}{dt^*_S}, \\ \dfrac{d\theta^*_{1_S}}{dt^*_S} = \dfrac{U^*_S \cos 2\theta^*_{1_S}}{8\rho^{*3}_{1_S}\cos\theta^*_{1_S}}, \end{cases} \tag{33}$$

with the initial conditions:

$$\begin{cases} \rho^*_{1_S}(0) = 0, & \\ \theta^*_{1_S}(0) = \theta^*_0, & \theta^*_0 \in (-\frac{\pi}{2}, \frac{\pi}{2}). \end{cases} \tag{34}$$

The initial condition for $\theta^*_{1_S}$ will be derived below because we do not know a priori the initial direction of the vortex.

We make the above system autonomous by introducing the following new variables:

$$\alpha = U^*_S\rho^{*3}_{1_S}, \qquad \beta = \sin\theta^*_{1_S}, \tag{35}$$

and

$$\bar{t} = \int_0^{t^*_S} U^{*2}_S(t')dt'. \tag{36}$$

Rewriting the above equations of motion in terms of these new variables we obtain:

$$\begin{cases} \dfrac{d\alpha}{d\bar{t}} = \dfrac{\beta}{4}, \\ \dfrac{d\beta}{d\bar{t}} = \dfrac{1-2\beta^2}{8\alpha}, \end{cases} \tag{37}$$

with the initial conditions:

$$\begin{cases} \alpha(0) = 0, \\ \beta(0) = \beta_0, \qquad\qquad \beta_0 \in (-1,1). \end{cases} \tag{38}$$

These equations describe the evolution of the system independently of all the flow parameters and consequently they represent a universal set of equations for this class of flows within the Brown and Michael's model.

As final step toward the exact solution, we combine together the above equations obtaining a second order equation for α only:

$$\frac{d^2\alpha^2}{d\bar{t}^2} = \frac{1}{16}. \tag{39}$$

The integration of this equation and the derivation of the solution for β are now trivial. Finally, after imposing the initial condition the solution has the following form:

$$\alpha = \pm\frac{\bar{t}}{2^{\frac{5}{2}}}, \qquad\qquad \beta = \pm\frac{\sqrt{2}}{2}, \tag{40}$$

where the sign has to be taken positive if the flow is from left to right and negative otherwise. Since we assumed initially $U_S^* \geq 0\ \forall t_S^* \geq 0$, we choose the positive sign. The solution for $\rho_{1_S}^*$ and $\theta_{1_S}^*$ is recovered simply by inverting the relationships (35). We obtain:

$$\rho_{1_S}^* = \left[\frac{1}{2^{\frac{5}{2}}U_S^*}\int_0^{t_S^*} U_S^{*2}(t')dt'\right]^{\frac{1}{3}}, \qquad\qquad \theta_{1_S}^* = \frac{\pi}{4}. \tag{41}$$

Note that $\theta_{1_S}^* = \pi/4$ identifies a universal trajectory, i.e., within this model the starting vortex leaves the tip of the plate and moves on a trajectory always perpendicular to the plate for any free-stream condition. This result substantiates the hypothesis that the vortices move on the same trajectory even in the finite plate case. We derive the circulation associated with the vortex using the polar form of expression (31). We obtain:

$$\Gamma_{1_S}^* = \pi U_S^*\left[\frac{1}{2U_S^*}\int_0^{t_S^*} U_S^{*2}(t')dt'\right]^{\frac{1}{3}}. \tag{42}$$

Consequently, the rate of circulation production has the following form:

$$\frac{d\Gamma_{1_S}^*}{dt_S^*} = \frac{\pi}{3}U_S^*\left[\frac{dU_S^*}{dt_S^*}\int_0^{t_S^*} U_S^{*2}(t')dt' + \frac{U_S^{*3}}{2}\right]\left[\frac{U_S^{*2}}{2}\int_0^{t_S^*} U_S^{*2}(t')dt'\right]^{-\frac{2}{3}}. \tag{43}$$

The last two results permit us to define the range of validity of the solution. The solution is physically valid $\forall t_S^* \geq 0$ only if the free-stream velocity is a monotonically increasing function of

time. Otherwise, if the flow is allowed to decelerate then the rate of circulation production might change sign and hence the solution is valid only up to time t^*_{shed} when $\frac{d\Gamma^*_{1S}}{dt^*_S} = 0$. To analyze this situation we assume that the free-stream velocity is a monotonically increasing function of time (i.e., $\frac{dU^*_S}{dt^*_S} > 0$) up to t^*_{max} where it reaches its maximum (i.e., $\frac{dU^*_S}{dt^*_S} = 0$) and then it becomes a monotonically decreasing function of time (i.e., $\frac{dU^*_S}{dt^*_S} < 0$) up to t^*_{final} when it becomes zero. Then, for such a free-stream velocity the above solution is mathematically, but not physically, well defined. In fact, from the expression for Γ^*_{1S} it follows that the sign of the circulation agrees with the sign of the free-stream velocity and it goes to zero at t^*_{final}. Consequently, the strength of the vortex increases at the beginning, then it reaches a maximum, then starts to decrease and finally the circulation vanishes. This behavior is unphysical for $t^*_S > t^*_{shed}$, i.e., when the vortex circulation is decreasing. In other words, at time t^*_{shed}, when the rate of circulation production changes sign, the simulation should be stopped and a new vortex introduced in the flow (see Cortelezzi and Leonard 1993) for an application of this shedding mechanism). It is interesting to predict when this happens. The expression (43) shows that the sign of the rate of circulation production depends on the sign of the free-stream acceleration. Then, $\frac{d\Gamma^*_{1S}}{dt^*_S}$ is positive up to time t^*_{max}, because $\frac{dU^*_S}{dt^*_S} \geq 0$, and negative at time t^*_{final}, because $\Gamma^*_{1S} = 0$, it follows that $t^*_{max} < t^*_{shed} < t^*_{final}$. Hence, the rate of circulation production changes sign always during the flow deceleration or, in other words, the system starts to produce circulation of opposite sign before the flow is actually reversed. The time t^*_{shed} when the rate of circulation production goes to zero depends on free-stream velocity and in principle can always be computed by solving the following equation:

$$\left.\frac{dU^*_S}{dt^*_S}\right|_{t^*_S = t^*_{shed}} = -\frac{U^{*3}_S(t^*_{shed})}{2}\left[\int_0^{t^*_{shed}} U^{*2}_S(t')dt'\right]^{-1}. \tag{44}$$

The case where the free-stream velocity has more than one maximum is physically ambiguous because we do not know how many vortices are actually created. The solution is mathematically well defined but its physical meaning depends on the particular situation under investigation.

5.1.3 Scaling and Universality

The exact solution (40) is a universal solution for the unsteady separated flow past a semi-infinite plate within this model. In other words, given the solution (40) we can derive the exact solution for any given free-stream condition. The only drawback is that the quantities α and β do not have a direct physical meaning. The possibility of a better scaling is suggested by the form of the above solutions (41) and (42). Let us introduce the following scaled quantities:

$$\begin{aligned} \rho^\bullet_{1S} &= \rho^*_{1S}, \qquad \theta^\bullet_{1S} = \theta^*_{1S}, \qquad t^\bullet_S = \frac{1}{U^*_S}\int_0^{t^*_S} U^{*2}_S(t')dt', \\ U^\bullet_S &= \frac{U^*_S}{U^*_S} = 1, \qquad \Gamma^\bullet_{1S} = \frac{\Gamma^*_{1S}}{U^*_S}. \end{aligned} \tag{45}$$

Then, the rate of circulation production has the following form:

$$\frac{d\Gamma^{\bullet}_{1_S}}{dt^{\bullet}_S} = \frac{1}{U^{*2}_S}\left[\frac{d\Gamma^{*}_{1_S}}{dt^{*}_S} - \frac{\Gamma^{*}_{1_S}}{U^{*}_S}\frac{dU^{*}_S}{dt^{*}_S}\right]\left[1 - \frac{1}{U^{*3}_S}\frac{dU^{*}_S}{dt^{*}_S}\int_0^{t^{\bullet}_S} U^{*2}_S(t')dt'\right]^{-1}. \tag{46}$$

Rewriting the exact solution (41–43) in terms of these scaled quantities we obtain:

$$\rho^{\bullet}_{1_S} = \frac{t^{\bullet\frac{1}{3}}_S}{2^{\frac{5}{6}}}, \qquad \theta^{\bullet}_{1_S} = \frac{\pi}{4}, \tag{47}$$

and the circulation and its rate of production become:

$$\Gamma^{\bullet}_{1_S} = \pi\left(\frac{t^{\bullet}_S}{2}\right)^{\frac{1}{3}}, \qquad \frac{d\Gamma^{\bullet}_{1_S}}{dt^{\bullet}_S} = \frac{\pi}{3}\frac{1}{(2t^{\bullet 2}_S)^{\frac{1}{3}}}. \tag{48}$$

This is, again, a universal solution, because does not depend on the free-stream velocity but has a greater physical meaning because it coincides with the exact solution for the impulsively started case when the free-stream velocity is unit. Consequently, within this model, the knowledge of the behavior of the system for the impulsively started case is sufficient to produce complete information about any other case.

5.2 Finite Plate Scaling

The analysis of the Figures 6a-d show that all the curves for a given flow quantity are similar and consequently it might exist a global time scaling able to collapse all the curves onto one. In particular, Figure 7 shows that the merging process is completed always at about the same bubble length, independently of the power-law, hence an appropriate time scaling might be able to synchronize the diamond symbols.

The time scaling derived in the previous subsection for the semi-infinite plate it must hold, at very early times, for the starting flow past a finite plate. In particular when the free-stream velocity has a power-law form the scaled time (45) reduces to:

$$t^{\bullet}_S = \frac{t^{*(m+1)}_S}{2m+1}. \tag{49}$$

If we now compare the above time scale valid for small times with the time scale valid for large times (25) we see that the difference is just a multiplicative factor. For small times is $1/(2m+1)$ instead for large times we have $1/(m+1)$. Based on these observations one might argue that a global scaling could have the following form:

$$t^{\bullet} = \frac{t^{*(m+1)}}{2m+1-mf^{*}(t^{*})}, \tag{50}$$

where the dimensionless function f^{*} has to satisfy the following constraint:

$$\lim_{t^{*}\to 0} f^{*}(t^{*}) = 0, \qquad \lim_{t^{*}\to\infty} f^{*}(t^{*}) = 1, \tag{51}$$

or, in other words, $t^\bullet \sim t_S^\bullet \ \ \forall t^\bullet \ll 1$ and $t^\bullet \sim t_L^\bullet \ \ \forall t^\bullet \gg 1$. Then the scaling of the equation of motion (12) for the power-law case is carried out using the quantities defined in (25) where the dimensionless time $t^\bullet$ now replaces $t_L^\bullet$. We do not report the expression of the scaled equation of motion because its mathematical expression does not provide any insight about the universality achievable. As before the quantities which involve time derivatives have a non trivial and rather unusual expression. Let g represent Γ_1 or I, then the expression for the scaled rate of circulation production and drag can be obtained from the following formula:

$$\frac{dg^\bullet}{dt^\bullet} = \frac{(2m+1-mf^*)^2}{t^{*2m}} \left[\frac{dg^*}{dt^*} - \frac{mg^*}{t^*}\right] \left[(m+1)(2m+1-mf^*) + mt^* \frac{df^*}{dt^*}\right]^{-1}. \tag{52}$$

Note for $m = 0$ we are, once again, recovering the geometrical scaling (11).

We were not able to derive a function f^* such that satisfies the constraints (51) and that produces a global scaling probably because of the error which affects the simulation for large times. Consequently, we concentrated on the scaling of the early times of the flow, i.e., up to the time when the plate has traveled few plate lengths. In the attempt to extend the time scaling valid at small times we assume that the function f^* has the following polynomial form:

$$f^*(t^*) = C_{1m} t^{*\frac{2(m+1)}{3}} + C_{2m} t^{*(m+1)}. \tag{53}$$

where, the coefficients C_{m1} and C_{m2} are evaluated numerically and have the following values:

m	C_{1m}	C_{2m}
1	.125174	−.054214
2	.087456	−.025007
5	.054764	−.009961
10	.036116	−.005251

Clearly this function satisfies only the constraint at $t^* = 0$, nevertheless, it produces the desired collapse during the early times of the flow. Although not global the importance of this result is emphasized by the fact that experimentally the symmetry of the wake is lost on the same time scale.

Figures 8 and 9 show the results of the scaled simulation up to time $t^\bullet = 16$, when the plate has traveled about four diameters. The overall effect of the scaling is to nearly collapse all the curves obtained for different power-laws onto the corresponding curve for the impulsively started case, i.e., $m = 0$. Figures 8b and 8d show that the scaling appears to break-down at $t^\bullet \sim 12$ when the curves for the rate of circulation production and the drag start to fan out. The phenomenon is almost negligible for all the other quantities (see Figures 8a, 8c, and 9). The drag and the rate of circulation production are the first quantities which show the limit of the scaling probably because their scaled form (52) is rather complex, involving both f^* and its time derivative. The above results show that, within this inviscid model and under this scaling, the power-law starting flow has an universal behavior, i.e., all the case are nearly the same up to time $t^\bullet \sim 12$. In other words, it is enough to study the evolution of the system for a given power-law to obtain information about the evolution of the system for any other power-law.

The possibility of extending these results to the viscous case is an open and challenging question. If this were the case it would suffice to perform a careful experiment for a given power-law to obtain

information about any other case. Furthermore, it would open a way to better compare numerical simulation and theoretical prediction with experimental result. For example, the theoretical prediction for the impulsively started case could be compared with the experimental data obtained by towing the plate at some convenient constant acceleration. The extension of the above results to the viscous case is non trivial but indication that a scaling might exist is given by the results obtained by Taneda and Honji[4]. In fact, the time-laws for the impulsively started (16) and for the constantly accelerated (17) cases might be scaled in the following way:

$$\frac{L_{bbl}}{L} = .89\ t_{TH}^{\bullet\frac{2}{3}} \tag{54}$$

where

$$t_{TH}^{\bullet} = \frac{2Vt^{m+1}}{(3m+2)L}, \qquad m = 0, 1. \tag{55}$$

Note the multiplicative factor .48 in expression (17) is recovered exactly to its two digits precision. An interesting point is that the time scaling (25) for the point vortex model and the experiment differs by a multiplicative factor. Such a difference is anyway not surprising because in the real flow the vorticity is distributed along the shear layer while, in the point vortex model, the circulation is lumped in one point.

6 Conclusions

An irrotational model has been used to model the power-law starting flow past a flat plate. Using dimensional analysis the problem is made dimensionless recovering dynamical similarity for a given power law. The model has been tested simulating the unsteady separated flow past a plate when the free-stream velocity is a step, a ramp or a parabolic function of time and then has been successfully validated by matching the results obtained both numerically and experimentally. The results of these simulations suggested the existence of a further time scaling. A time-dependent scaling has been obtained by synchronizing the motion of the plate for different time laws. Under this scaling the equation of motion became asymptotically independent of all the flow parameters and hence universal for large times. The recomputed simulations produced for each flow quantity a family of curves which allows one to compare the results obtained for different power-laws. The analysis of these families of curves showed sign of universality even at early times. We first analyzed the behavior at small times by exactly solving and scaling the corresponding flow past a semi-infinite plate. Then, we generalized this result to the finite plate case and derived a time-dependent scaling valid at early times. The new time scaling collapsed all the results onto the corresponding curve obtained for the impulsively started case. Under this scaling the power-law starting flow exhibited a universal behavior up to the time when the plate has traveled about four diameters. Finally, the existence of a global scaling and the possible extension of these results to the viscous case are discussed.

7 Acknowledgments

The author wishes to thank Dr. A. Leonard, Dr. A. Roshko, and Dr. D.E. Auerbach for several valuable discussions. This work was supported by the Office for the Naval Research Grant #N00014-90-J-1589.

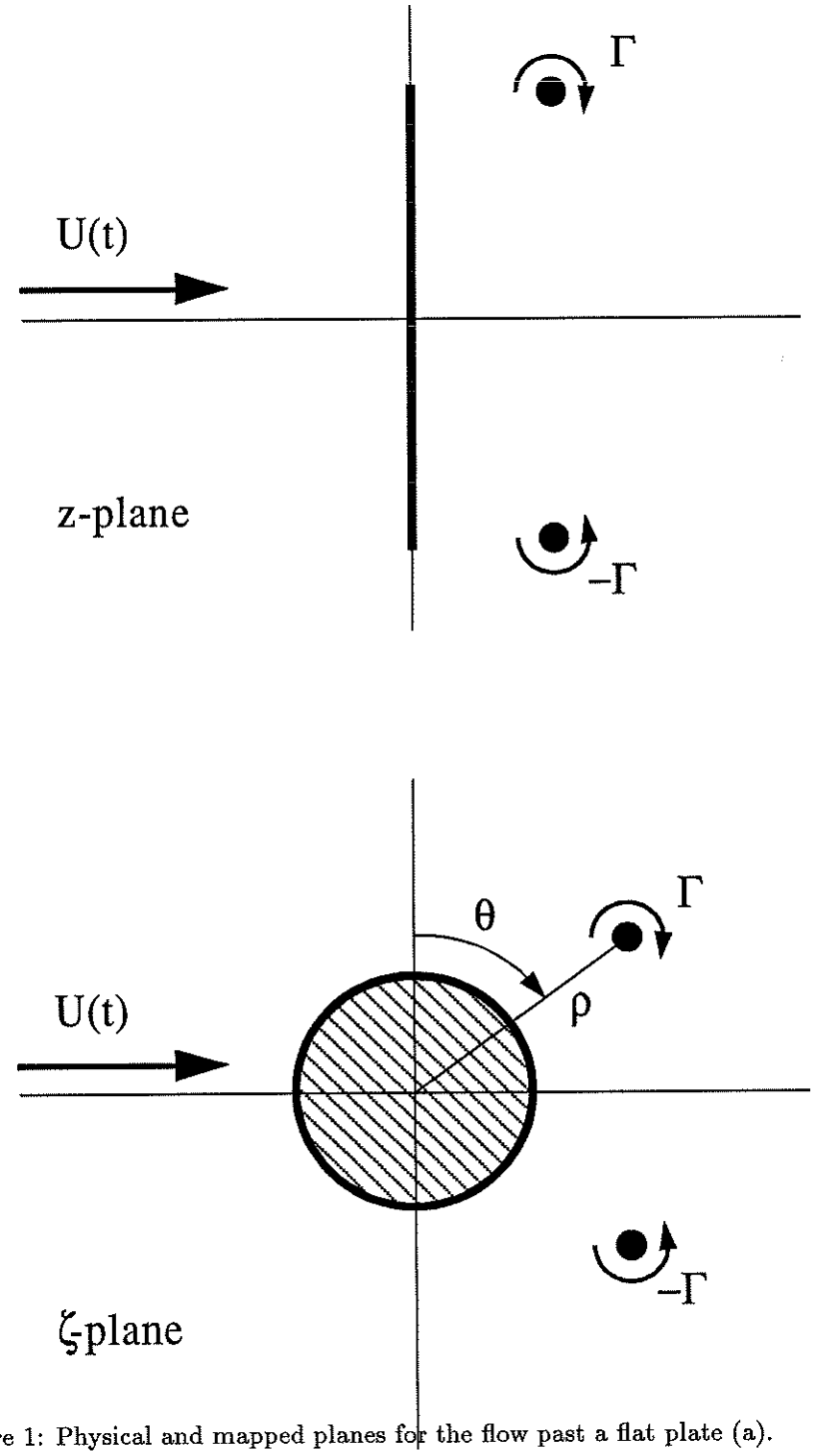

Figure 1: Physical and mapped planes for the flow past a flat plate (a).

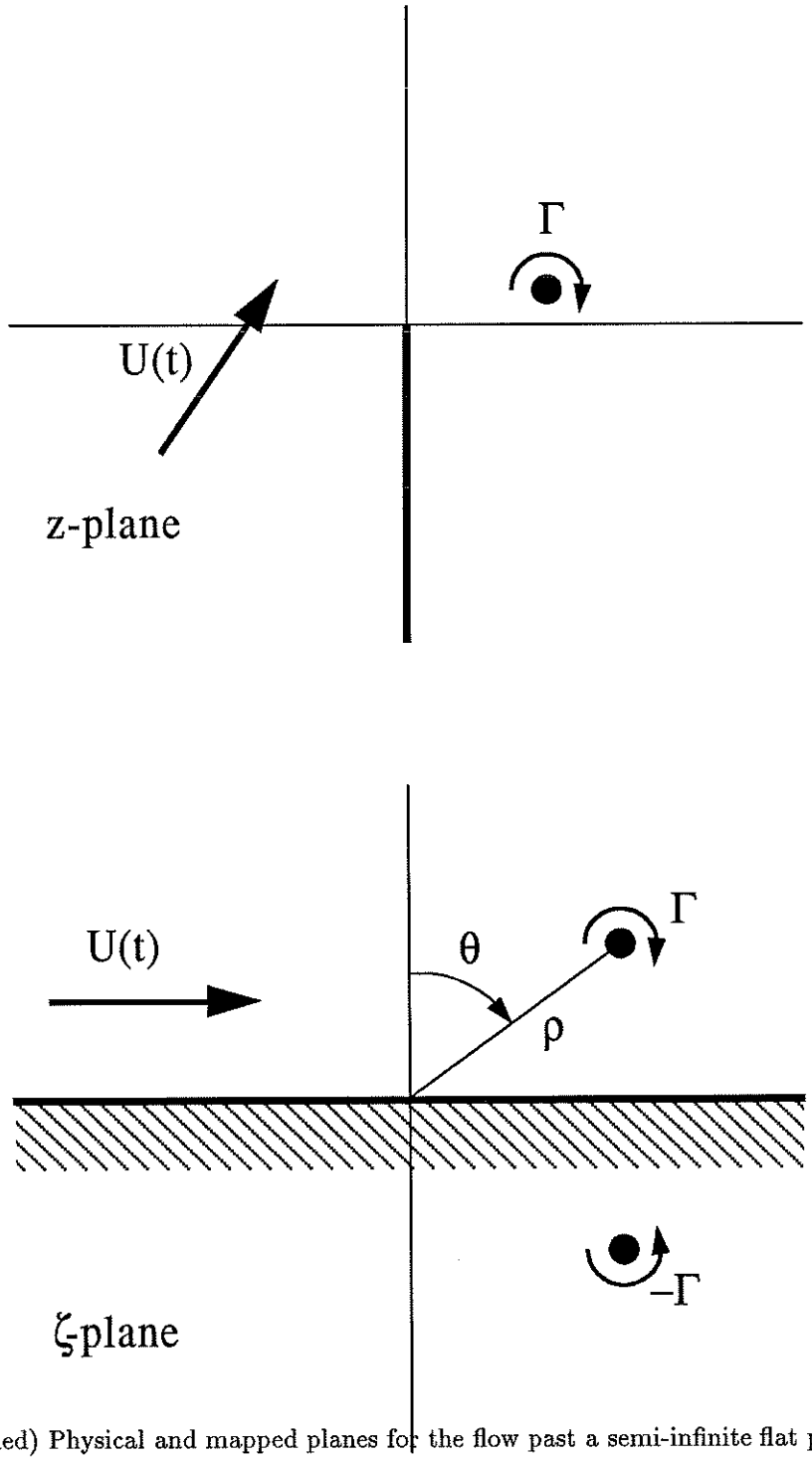

Figure 1: (Continued) Physical and mapped planes for the flow past a semi-infinite flat plate (b).

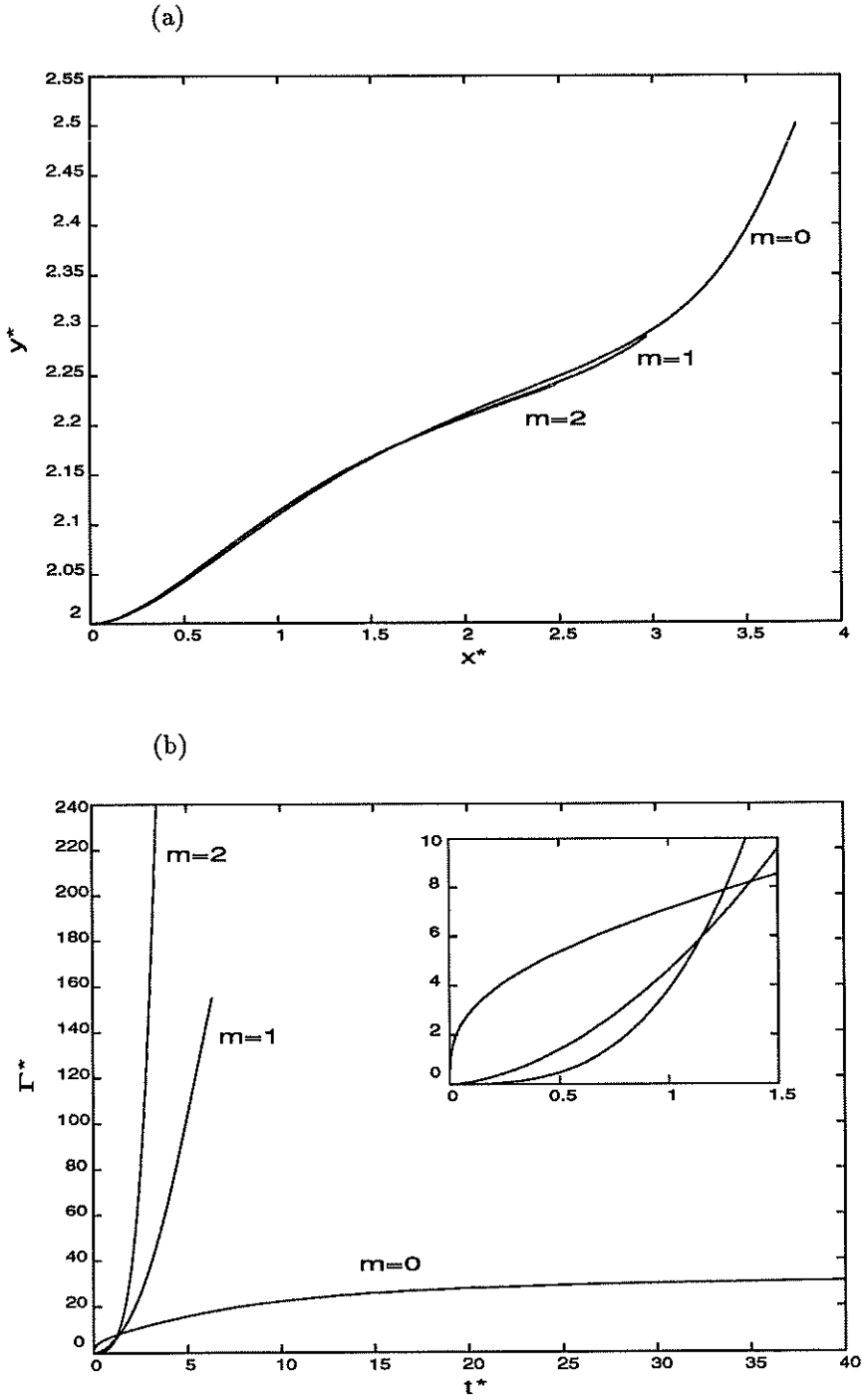

Figure 2: Trajectories of the top vortex (a) and total circulation of the top vortex (b) ($m = 0, 1, 2$).

(c)

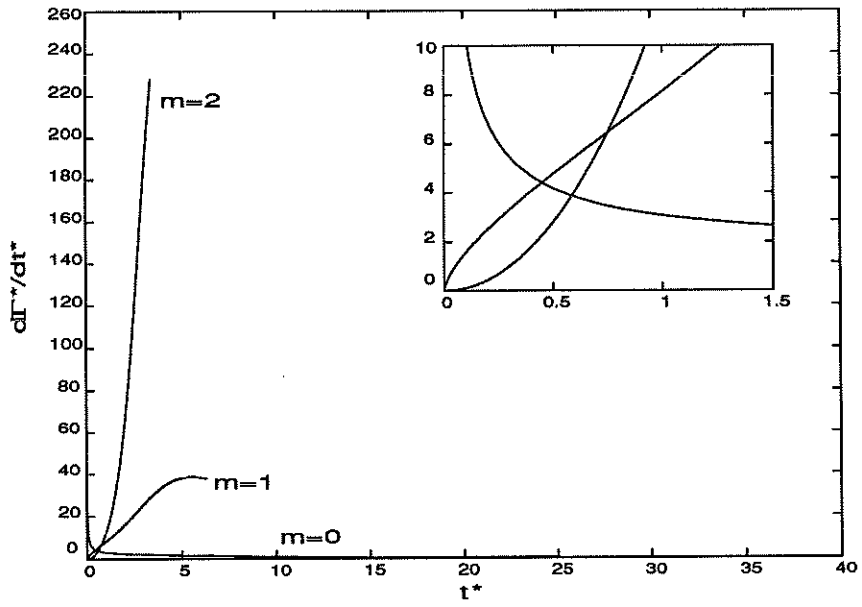

(d)

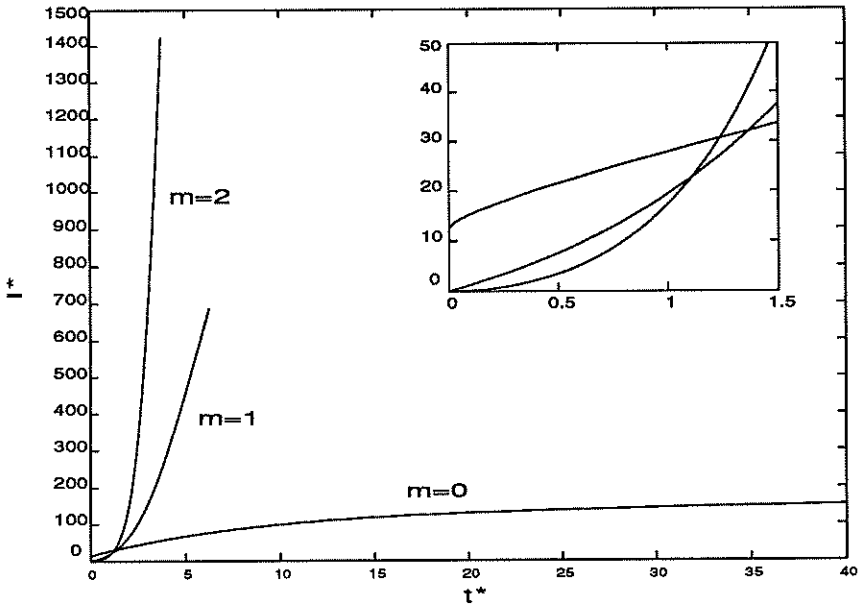

Figure 2: (Continued) Rate of circulation production for the top vortex (c) and and total impulse (d) ($m = 0, 1, 2$).

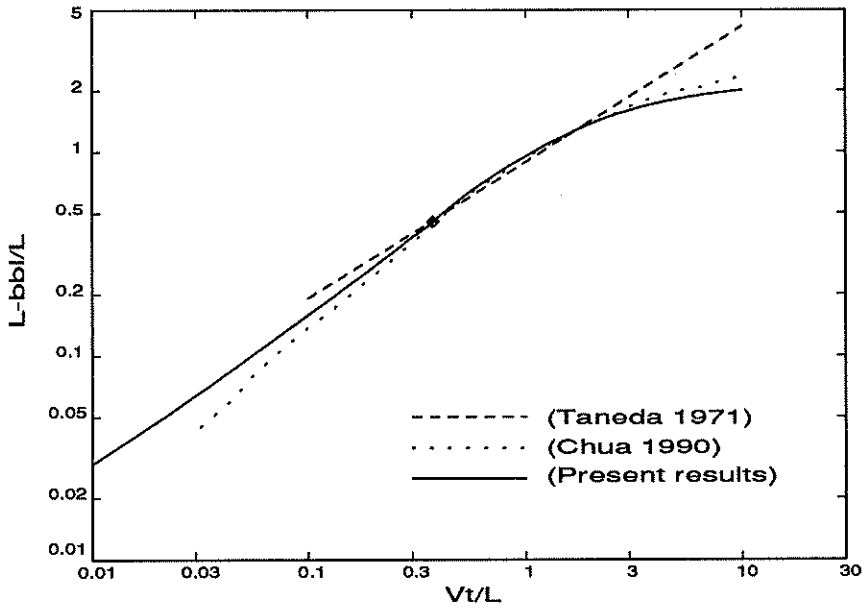

Figure 3: Length of the recirculating bubble, a comparison.

(a)

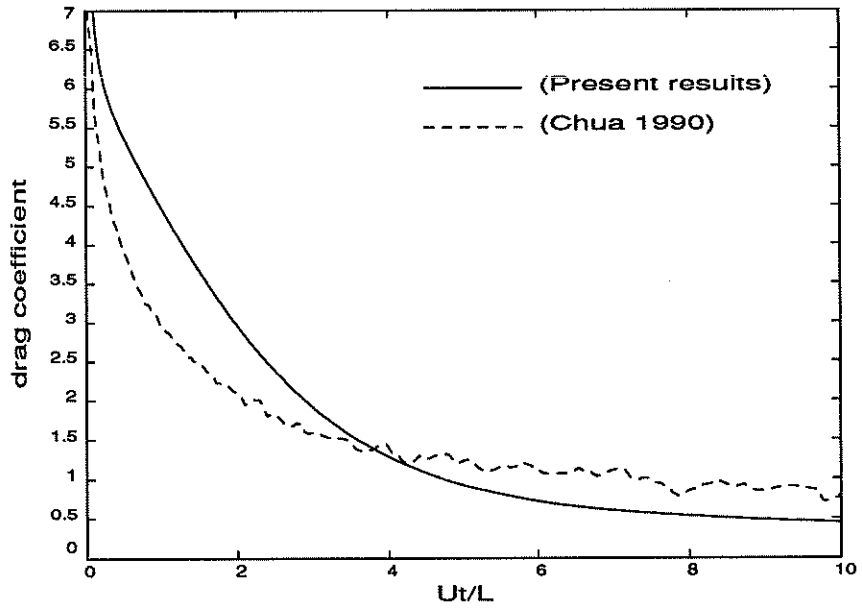

(b)

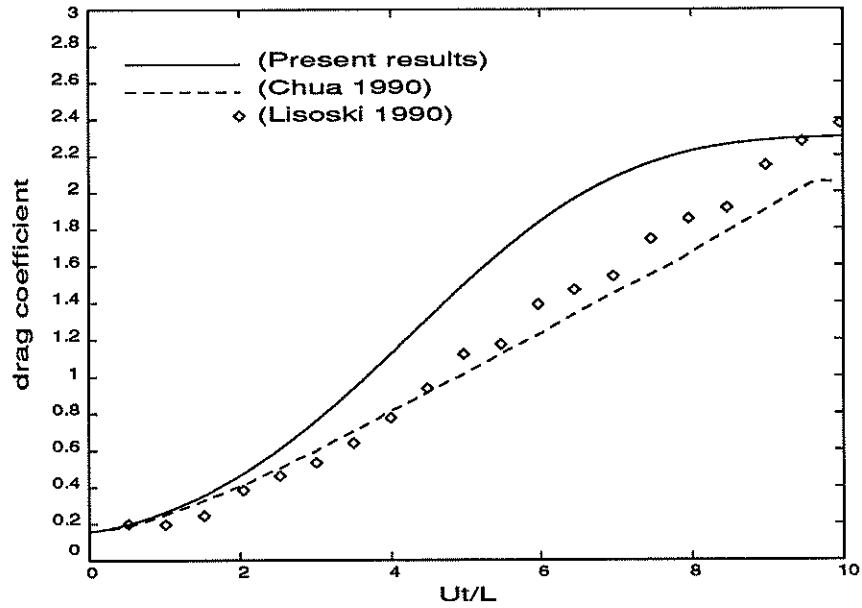

Figure 4: Drag coefficient comparison for the impulsively started (a, $m = 0$) and constantly accelerated plate (b, $m = 1$).

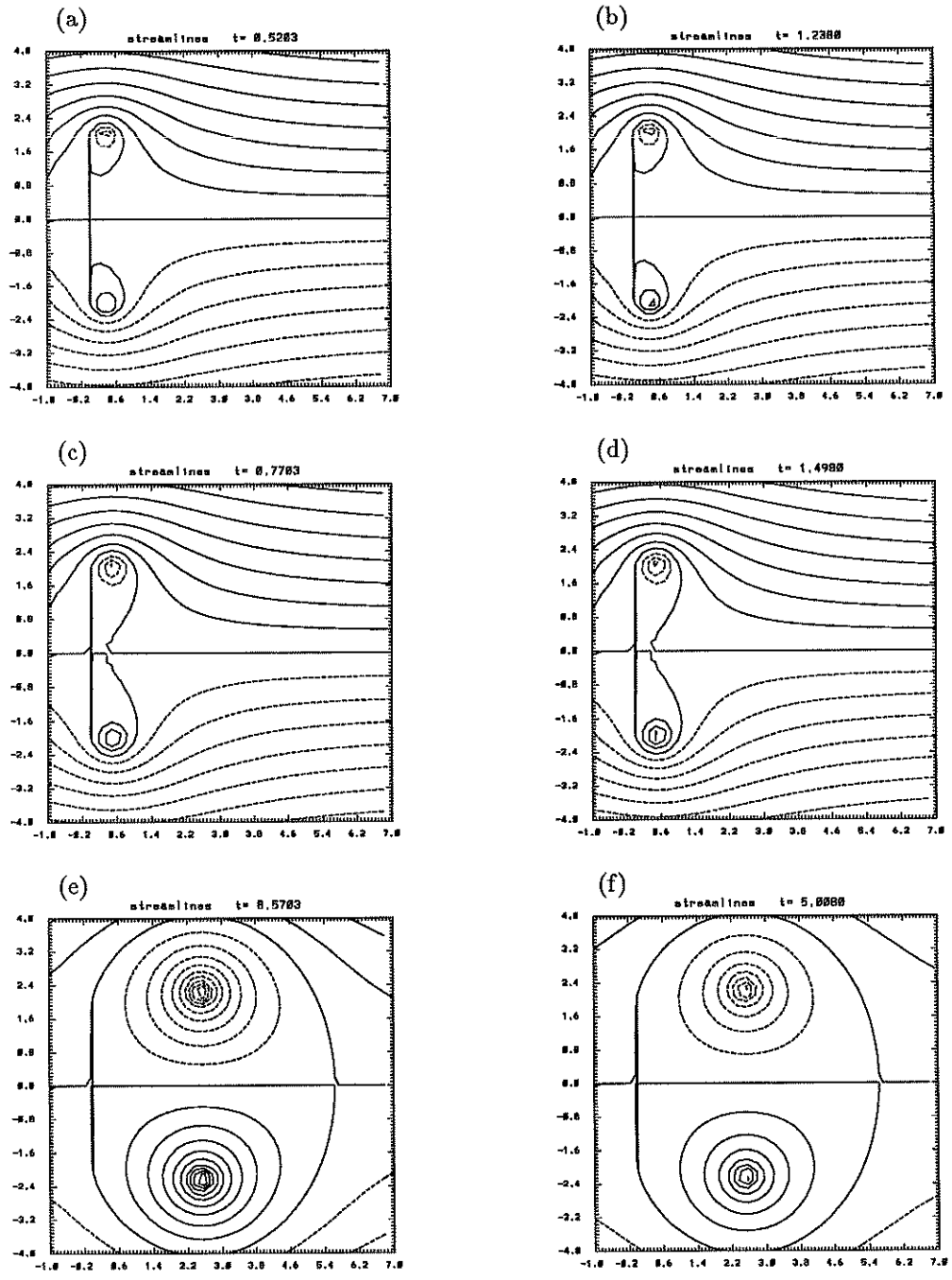

Figure 5: Instantaneous streamlines for the impulsively started case (m=0, t=0.52(a), 0.77(c), 8.57(e)) and for the constantly accelerated case (m=1, t=1.24(b), 1.50(d), 5.01(f)).

(a)

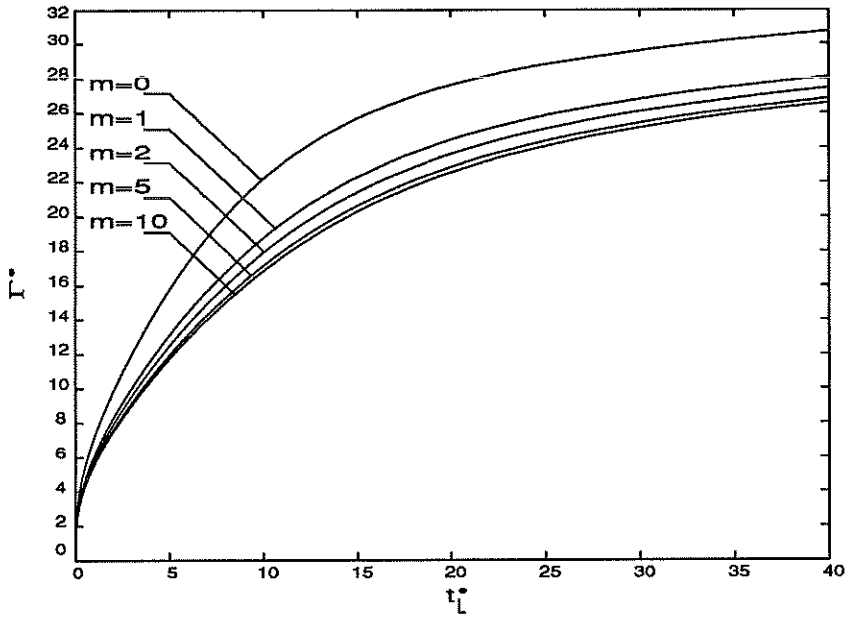

(b)

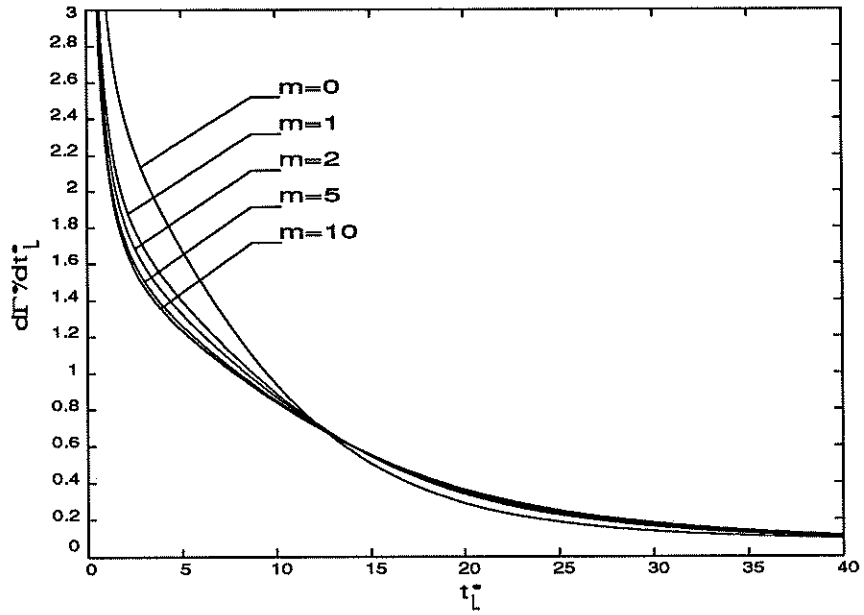

Figure 6: Total circulation of the top vortex (a) and rate of circulation production for the top vortex (b) ($m = 0, 1, 2, 5, 10$).

(c)

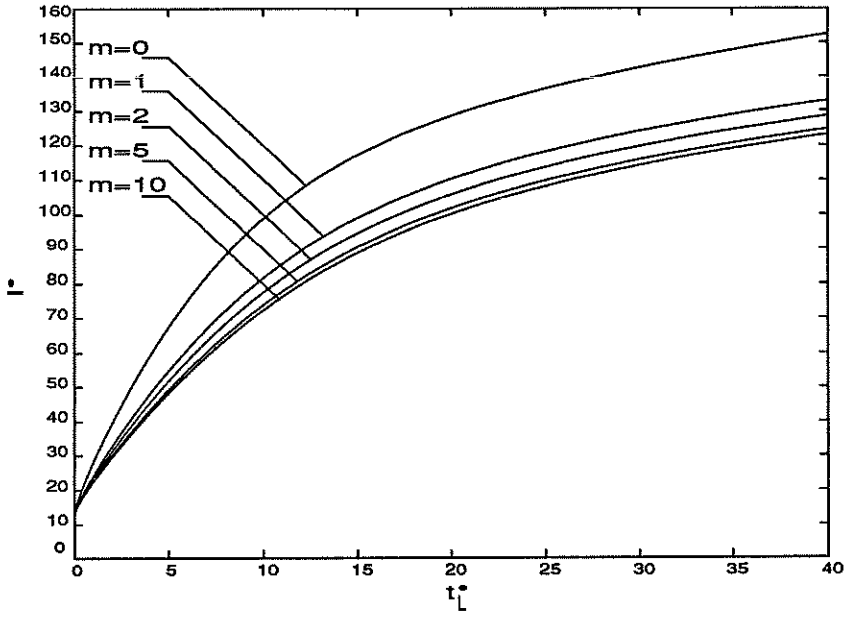

(d)

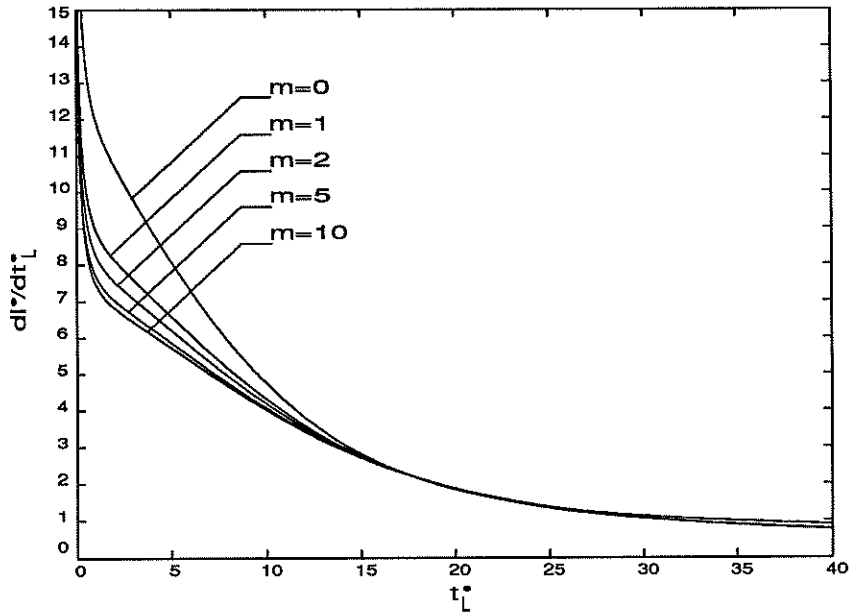

Figure 6: (Continued) Total impulse (c) and drag (d) ($m = 0, 1, 2, 5, 10$).

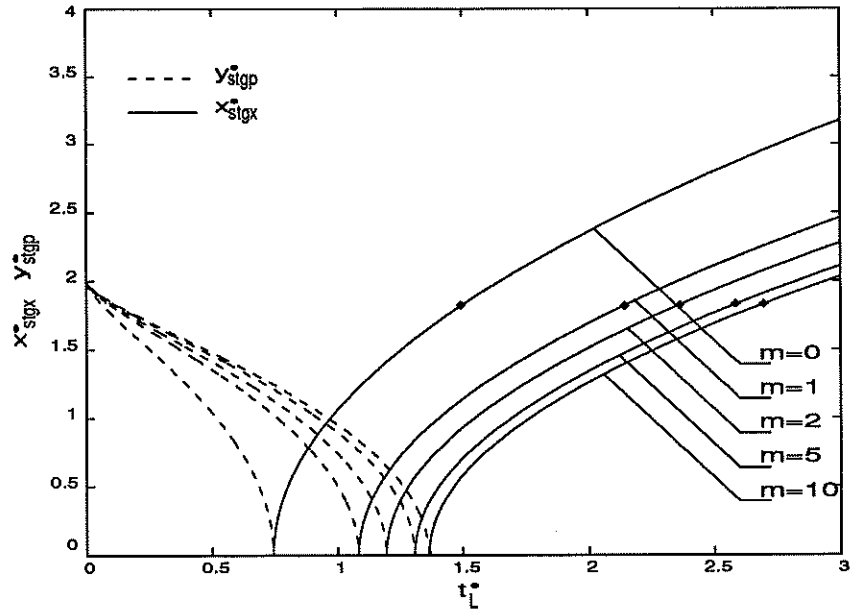

Figure 7: Loci of the stagnation points ($m = 0, 1, 2, 5, 10$).

(a)

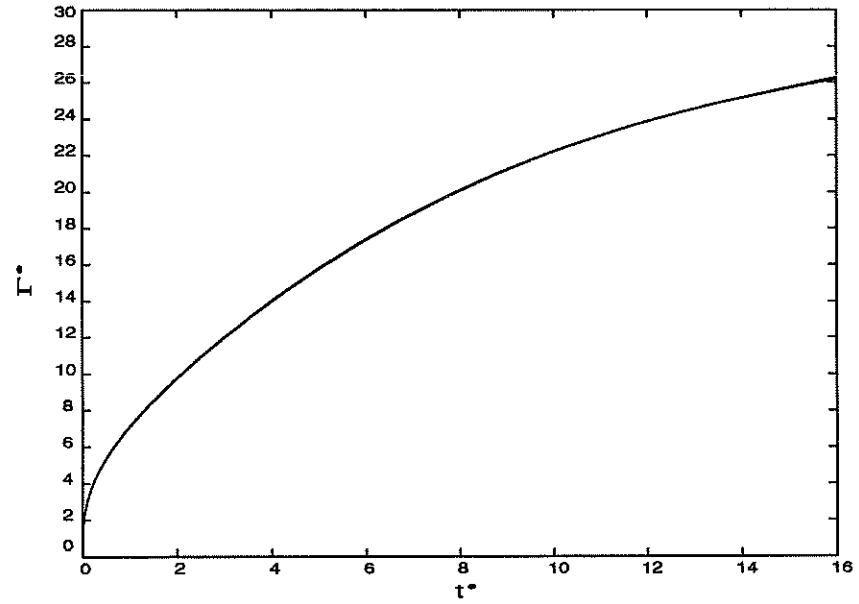

(b)

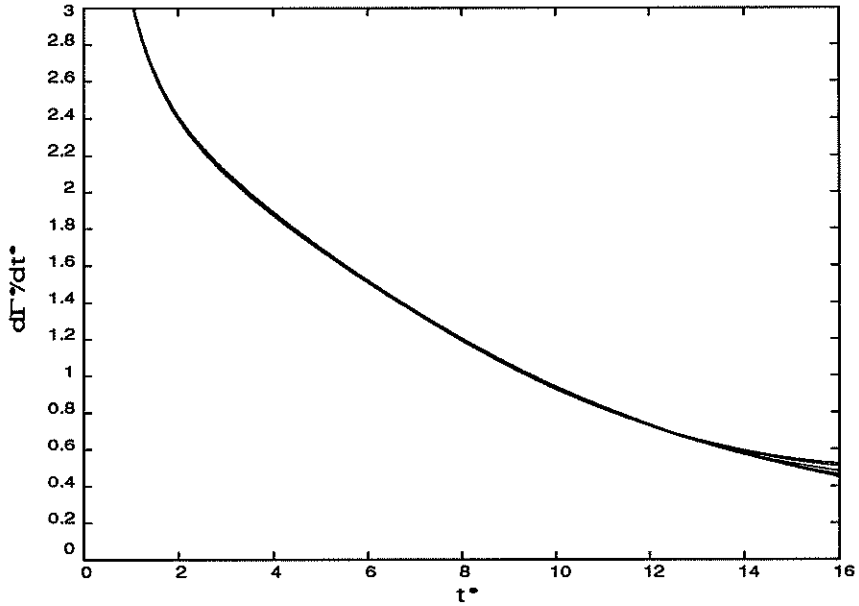

Figure 8: Total circulation of the top vortex (a) and rate of circulation production for the top vortex (b) ($m = 0, 1, 2, 5, 10$).

(c)

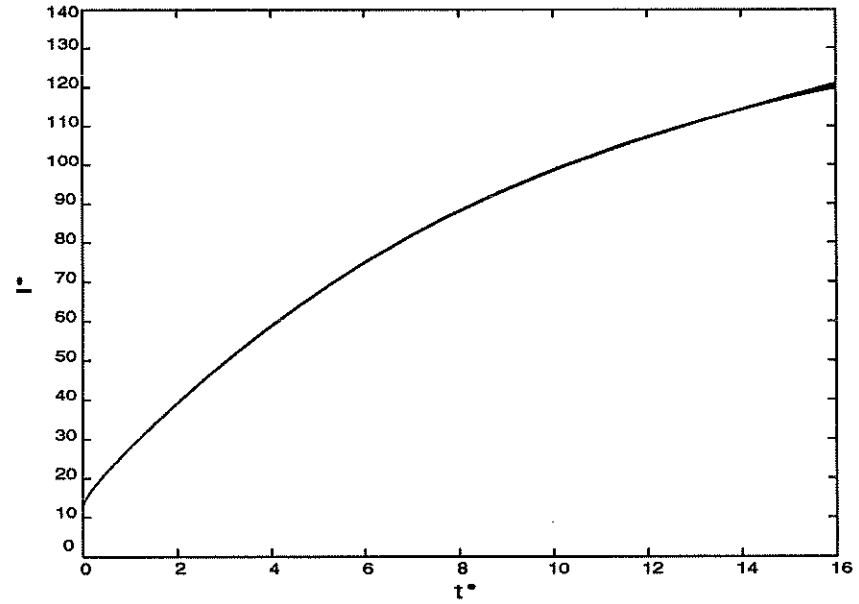

(d)

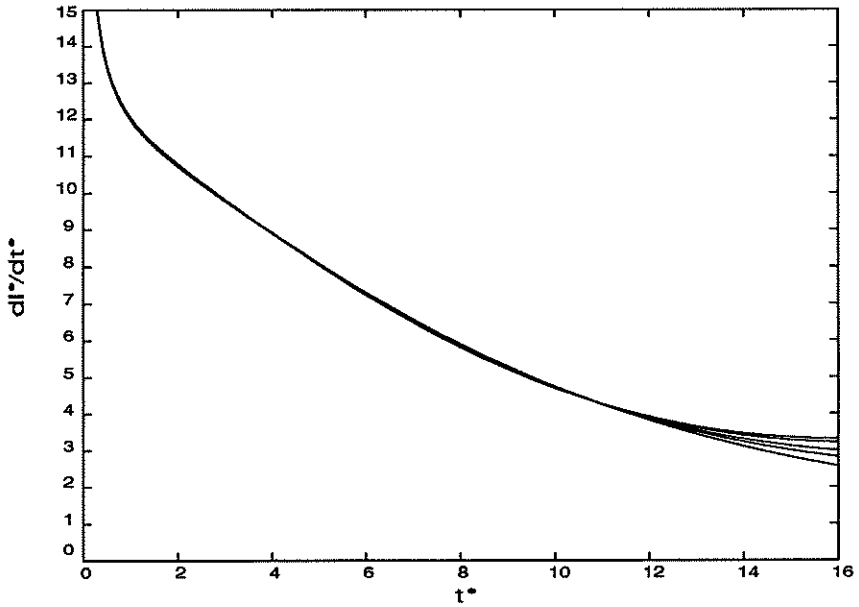

Figure 8: (Continued) Total impulse (c) and drag (d) ($m = 0, 1, 2, 5, 10$).

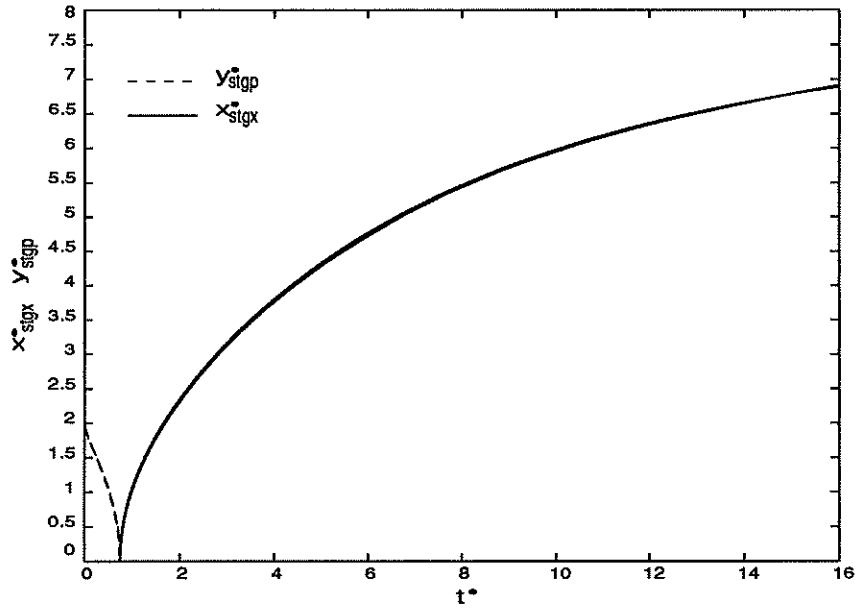

Figure 9: Loci of the stagnation points ($m = 0, 1, 2, 5, 10$).

References

Brown, C.E. & Michael, W.H. 1954 Effect of leading-edge separation on the lift of a delta wing. *J. Aero. Sci.* **21**, 690–694.

Cheers, A.Y. 1979 A study of incompressible 2-d vortex flow past a circular cylinder. Lawrence Berkeley Laboratory LBL-9950.

Chua, K. 1990 Vortex simulation of separated flows in two and three dimensions. Ph.D. Thesis, California Institute of Technology.

Clements, R.R. 1973 An inviscid model of two-dimensional vortex shedding. *J. Fluid Mech.* **57**, 321–336.

Cortelezzi, L. & Leonard A. 1993 Point vortex model for the unsteady separated flow past a semi-infinite plate with transverse motion. *Fluid Dynamics Research* **11**, 263–295.

Graham, J.M.R. 1980 The forces on the sharp-edged cylinders in oscillatory flow at low Keulegan-Carpenter numbers. *J. Fluid Mech.* **97**, 331–346.

Lisoski, D.L. 1993 Nominally 2-dimensional flow about a normal flat plate. Ph.D. Thesis, California Institute of Technology.

Pullin, D.I. 1978 The large-scale structure of unsteady self-similar rolled-up vortex-sheets. *J. Fluid Mech.* **88**, 401–430.

Rott, N. 1956 Diffraction of a weak shock with vortex generation. *J. Fluid Mech.* **1**, 111–128.

Taneda, S. & Honji, H. 1971 Unsteady flow past a flat plate normal to the direction of motion. *J. Phys. Soc. of Japan* **30**, 263–272.